Enhancing Dielectric Properties through Nanocomposite Formation of Tripropylene Glycol Diacrylate and Montmorillonite"

Ahmed Benamor[a,B*], Ameur Ouali[a], Yazid Derouiche[c], M. Kharroubi[c], Lahcene Souli[d] Ulrich Maschke[e]

[a]Physics Department, Faculty of Science, University of M'sila, 28000 M'sila, Algeria.

[b]Laboratory of Physics, Physics Department, Faculty of Science, University of M'sila, 28000 M'sila, Algeria.

[c]Department of Physic, Faculty of Exact Sciences and Informatics, Ziane Achour University of Djelfa, Djelfa 17000, Algeria.

[d]Laboratory of Organic Chemistry and Natural Substances, Department of Chemistry, Faculty of Exact Sciences and Informatics, Ziane Achour University of Djelfa, Djelfa 17000, Algeria.

[e]Unité Matériaux et Transformations (UMET), UMR 8207–CNRS, Bâtiment C6, Université Lille 1 - Sciences et Technologies, 59655 Villeneuve d'Ascq Cedex, France.

[*]Corresponding author : E-mail: ahmed.benamour@univ-msila.dz

Received: 07/ 2023; Published: 08/ 2023

Abstract:

The study developed tripropylene glycol diacrylate/montmorillonite nano composites via in-situ physical cross-linking of TPGDA with different types of cationically exchanged montmorillonite. The cationic exchange was carried out using various chemical products as sources of cations. The synthesized nanocomposites were characterized by FTIR and XRD, and the dielectric properties of the TPGDA/MMt-Cs^+ composite were studied over a high frequency range of 12 to 200 MHz and at a temperature range of 293-373 K. The results showed that adding TPGDA to the montmorillonite material improved the AC conductivity, dielectric constant, tangent loss, and dielectric loss when compared to montmorillonite without additives.

Keyword: nanocomposites, montmorillonite, TPGDA, Dielectric analysis.

Tob Regul Sci. ™ 2023;9(1): 3938-3955
DOI: doi.org/10.18001/TRS.9.277

Introduction

Recently, the field of interest in silicate based composite materials has increased, with Many studies showing the advantage of merging polymers with clay that improved their mechanical [1-3], thermal [4,5] , electrical [6,7] or magnetic properties [8,9] ,and thus broadening their field of application.Of the known clays, there are montmorillonite belongs to the group of silicate minerals known as dioctahedral smectites. Structure of this kind of materials is formed by two tetrahedral sheets sandwiching an octahedral sheet. The tetrahedral sites are occupied by Si(IV) as a central atom while the octahedral ones contain Al(III) which can be substituted with Fe(III) or/and Mg(II). This kind of structure exhibits cation exchange properties and swelling ability [10–13] .They have been used in catalysts [14] ,medicine, cosmetic industry [15,16] ,biosensors [17,18] ,packaging materials[19,20] waste water treatment[21,22] and nanocomposites [23] .Tripropylene glycol diacrylate (TPGDA) contains two polymerizable acrylic groups per molecule, which enable it to form copolymers of, for example, acrylic or methacrylic acids and their salts, amides, esters, vinyl acetate and styrene. TPGDA is also an important feedstock for chemical syntheses because it readily enters into addition reactions [24,25] .The product can be polymerized by the usual bulk, solution, suspension and emulsion techniques. Removal of the stabilizer beforehand is generally unnecessary as its effect can be counteracted by an excess of initiator. Bulk polymerization is one of the most efficient processes for the production of inorganic-organic nanocomposites. In this case, the preparation of these materials consists of the Bulk polymerization of a monomer by the radical way in the presence of nano-sized mineral particles. The properties of the new material depend strongly on the interfacial interactions between the two phases brought into contact in the synthesis domain. A great deal of work has been carried out on bulk polymerization in the presence of particles of very varied natures.In this paper, tripropylene glycol diacrylate /montmorillonite nano composites were elaborated via in-situ physical cross-linking of TPGDA method with different type of cationically exchanged montmorillonite Li^+ , Na^+ , K^+ , Rb^+ , Cs^+ has been investigated using conductivity measurements, dielectric loss spectroscopy. Then the conductivity and dielectric properties of each sample were studied at a wide temperature range of 293 K to 473K. Furthermore, Jonscher's model is used for the study of ionic dc conductivity behavior.

Experimental

Materials

Tripropylene glycol diacrylate (TPGDA) (Sigma-Aldrich)used without further purification, Wyoming montmorillonite from the Crook Country deposit, Wyoming, USA (University, 915

West State Street, West Lafayette, source Clay Minerals Repository, SWy-2),RbCl, CsCl, KCl, NaCl(Sigma-Aldrich), are used as received, Sodium lauryl sulfate (sigma Aldrich), potassium peroxydisulfate (sigma Aldrich).

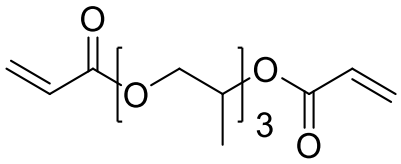

Figure 1. Chemical structure of Tripropylene glycol diacrylate TPGDA [24] .

Preparation of Montmorillonite-M^+ (M^+ = Rb, Cs, K, Na, Li)

30g of powdered montmorillonite was mixed with 1 liter of distilled water and 30 cc of hydrogen peroxide. The heterogeneous mixture was stirred for 2 hours at room temperature and then centrifuged for 20 minutes at 6000 rpm. The MMt was dried at 80°C for overnight. Then, 10g of crude clay is placed in a solution of MCl(M = Li, Na, K, Rb, Cs), (500ml, 1N) the suspensionwas stirred for 4 hours, then centrifuged for 15 minutes at 9000 rpm, this operation is repeated three times. The cationic exchanged montmorillonite was dried at 80°C.

Synthesis of cross-linking (tripropylene glycol diacrylate) /montmorillonite nanocomposites

5ml of TPGDA was mixed with 0.5g of montmorillonite in a round bottomed flask. The mixture was heated at 80°C with stirring about 120h. This time is considered long enough for the insertion of TPGDA in the interfoliar space of clay is complete. After 5 days,Then 0.25g of sodium lauryl sulfate was added to the mixture to form micelles and allow the reaction to proceed as polymerization with constant mechanical stirring. The TPGDA polymerization reaction was started with 0.0125 g of potassium peroxydisulfate for 4h at 80°C with constant stirring. The precipitate was washed thoroughly with methanol several times. Finally, the nanocomposite was then dried under vacuum.

Characterization

FT-IR spectrums were obtained byNicolet Avatar 330FT-IR Fourier Transform Interferometer over a range of 400 to 4000 cm^{-1} with a resolution of $2cm^{-1}$. The XRD patterns were obtained on an automated diffractometer (PW-1710, Philips) with a Cu tube that operated at 40 kV and 30mA. The diffractometer worked with a Xe-filled proportional counter and a diffracted beam curved graphite monochromator. The diffraction data were measured in the 2θ Bragg angle (range: 3– 70°), counting for 1s at every 0.02° step. The radiation used is copper Kα (λ = 1.54 Å). The conductivity δ_{ac},ωand dielectric permittivity (ε′) were measured using a Novocontrol Broad-band Dielectric Spectrometer (BDS 4000). The measurements havebeen performed at various temperatures from 293 K to 473 K by step 40 K and frequency (f) from 12Hz to

200MHz. In order to reach thermal equilibrium, the samples were maintained 30 minutes prior to experiments. The fine powder was compacted under 5.108Pascal (Pa) to obtain disc-shaped pellets (diameter = 10 mm, thickness = 1 mm).

Results And Discussion

X-ray diffractionanalysis

X-ray analysis of the treated montmorillonite, cross-linking (TPGDA)/ MMt-M^+ are presented in the (Fig.2).Firstly, the analysis clearly show that the cross-linking (TPGDA) was interposed between the montmorillonite-M^+ layers by forming nanocomposite materials.

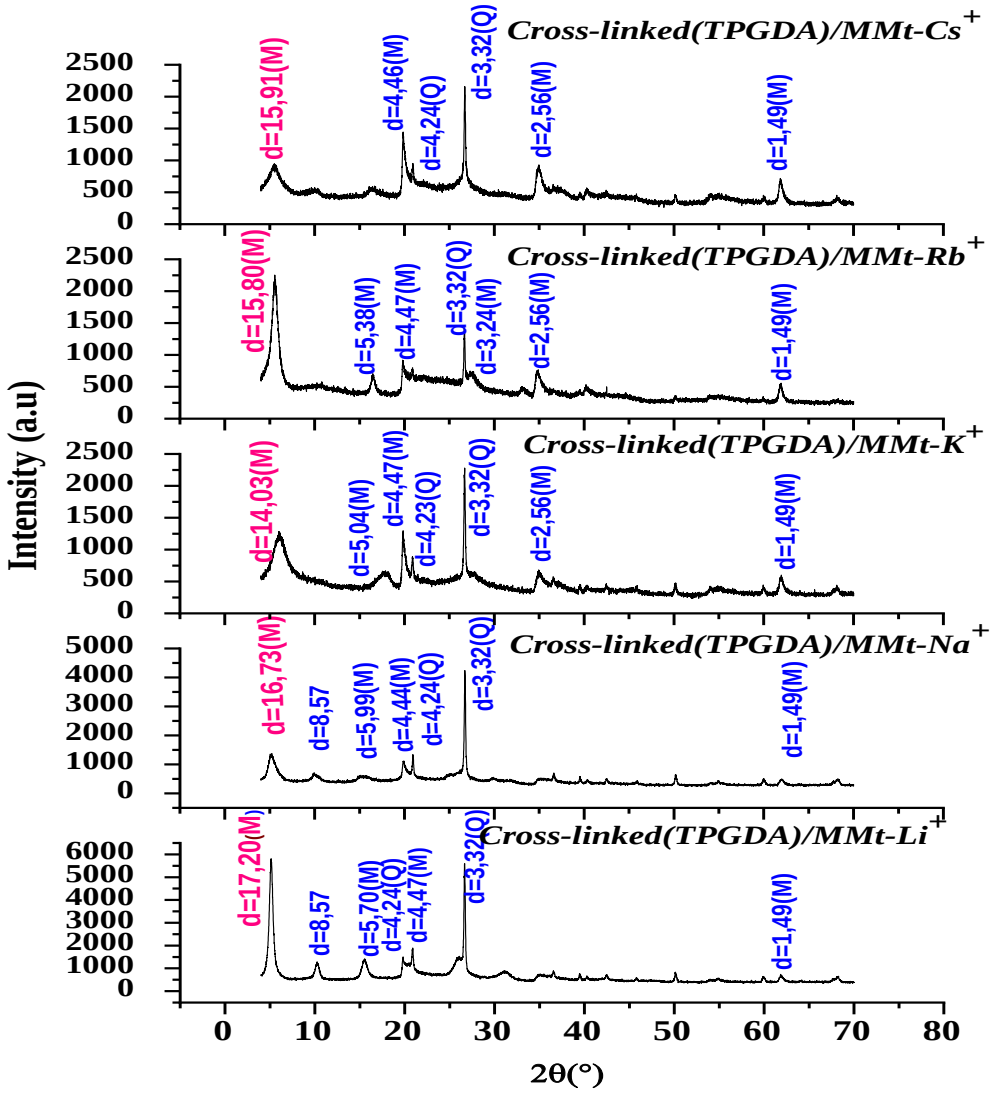

Figure 2. X-ray diffractograms of cross-linking (TPGDA)/MMt-M^+nanocomposite (M) refers to montmorillonite; (Q) refers to quartz.

There is a big difference between the spacing of nanocomposite scross-linked (TPGDA)/MMt-Li^+, cross-linked (TPGDA)/MMt-Na^+, cross-linked (TPGDA)/MMt-K^+, cross-linked (TPGDA)/MMt-Rb^+, cross-linked (TPGDA)/MMt-Cs^+.(Fig.3) is used to calculate the value of the basal spacing d_{001} in the sample nanocomposites. The values obtained are ordered as follows:d_{001}cross-linked(TPGDA)/MMt-Li^+>d_{001}cross-linked(TPGDA)/MMt-Na^+)>d_{001}cross-linked(TPGDA)/MMt-Cs^+)>d_{001}cross-linked (TPGDA)/MMt-Rb^+>d_{001} cross-linked (TPGDA)/MMt-K^+.

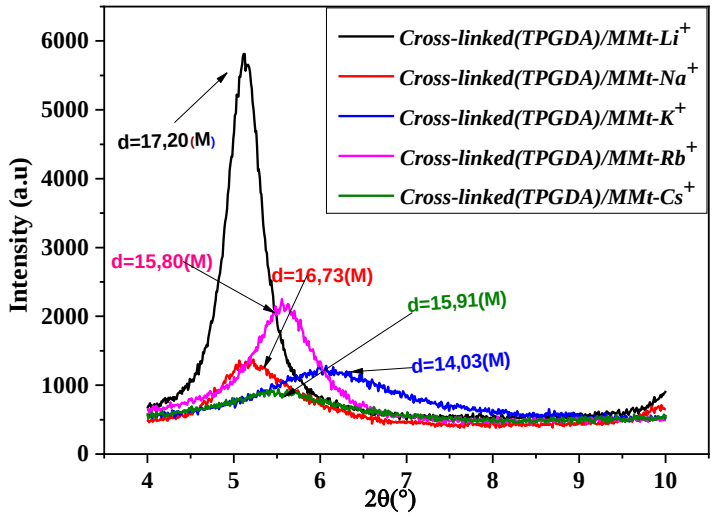

Figure 3. Comparison of the positions of (001) reflection peaks of cross-linking (TPGDA)/MMt-M^+ nanocomposite.

Small cations ($Li^+$and Na^+ for alkaline compensating cations) can easily be inserted into the hexagonal cavity, while the K^+cation follows the inhibitory potential [26] .

Table 1. The basal spacing for cross-linking (TPGDA)/MMt-M^+nanocomposite and ionic radius of the cations.

Sample	MMt-Li^+	MMt-Na^+	MMt-K^+	MMt-Rb^+	MMt-Cs^+
d_{001}(Å) MMt-M^+	11.9	11.4	11.08	11.82	12.19
d_{001}(Å) MMt-M^+& TPGDA	17.2	16.73	14.03	15.80	15.91
Ionic radius (Å)	0.6	0.95	1.33	1.48	1.69

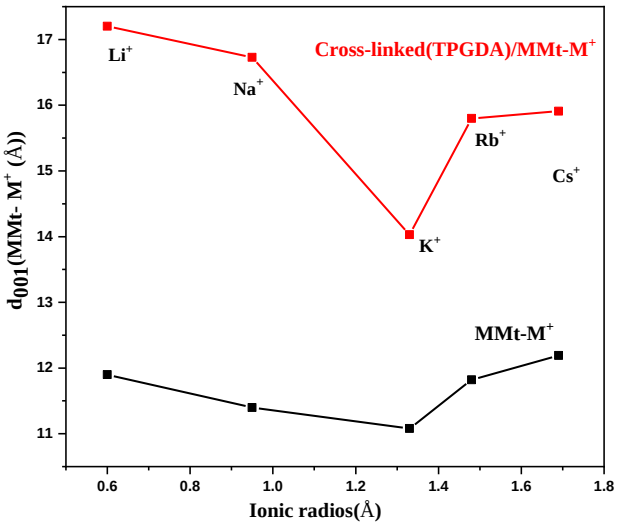

Figure 4. The basal spacing variation of a cross-linking (TPGDA)/MMt-M^+ nanocomposite as a function of the ionic radius.

Fourier Transform Infrared Spectroscopy (FTIR) analysis

The FT-IR spectra of MMt-$M^+$are represented in Fig.5.The band located at 3640 cm^{-1} corresponds to the vibrations of elongation of the OH groups of the Al-Al-OH octahedral layer. The band located at 3450 cm^{-1}characterizes the deformation vibrations of H_2O [27] .As well as the band of 1640 $cm^{-1}$is attributed to the vibrations of hydroxide of the adsorbed water. The intense band centered at 1050 cm^{-1} corresponds to the valence vibrations of the Si-O-Si bond [28] .In addition, the division of the OH group between the atoms Fe and Al and Mg in the octahedral position can shift the vibrations Al-OH towards the low frequencies around 815 and 915 cm^{-1}. 914.2 cm^{-1}corresponds to Al-Al-OH [29] .848.6 $^{cm-1}$corresponds to Al-Mg-OH [28] .The weak band 796 cm^{-1} is attributed to the vibrations of quartz. 514 cm^{-1}, 465 and 425 cm^{-1}, fixation of Si-O-Al deformation vibration [30] .We also note on the FT-IR spectra of cross-linking(TPGDA)/MMt-Li^+, cross-linking(TPGDA)/MMt-Na^+, cross-linking(TPGDA)/MMt-K^+, cross-linking(TPGDA)/MMt-Rb^+, cross-linking (TPGDA)/MMt-Cs^+ that bands around 2974 cm^{-1} and 2863 cm^{-1}have been allocated to the asymmetric stretch and symmetrical stretch vibrations of the $–CH_2$ group of TPGDA [31] .The absorption band at approximately 1715 cm^{-1}reflected the stretching vibration of the C = O group and the absence of the characteristic band of the CH_2 = C bond, which confirms the radical polymerization of TPGDA.

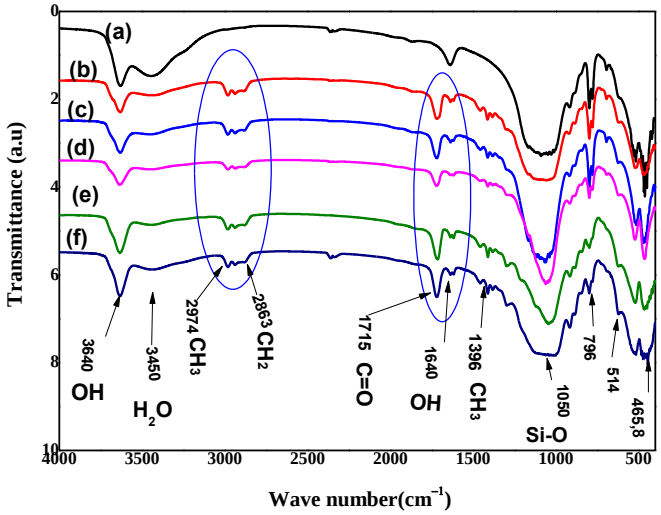

Figure 5. FTIR spectra of : (a) MMt-Na$^+$, (b) cross-linking (TPGDA)/MMt-Li$^+$nanocomposite, (c) cross-linking (TPGDA)/MMt-Na$^+$nanocomposite,(d) cross-linking (TPGDA)/MMt-K$^+$nanocomposite , (e) cross-linking (TPGDA)/MMt-Rb$^+$nanocomposite and(f) cross-linking (TPGDA)/MMt-Cs$^+$ nanocomposite.

Impedance Measurements

Conductivity spectrum

Fig.6 shows the evolution of the σ_{dc} conductivity spectra, σ_{dc} as a function of angular frequency (ω) for the frequency-dependent conductivity δ(ω)for cross-linking (TPGDA)/MMt-Cs$^+$ nanocomposite for different temperatures. For all temperatures, δ(ω)is independent of ω in low frequency regions and almost equal to the direct-current (σ_{dc}) conductivity. Then, the ac conductivity starts to increase. This trend in conductivity is similar to common electrical behavior of disordered materials. Almost all the composites show similar behavior up to[21444-185573]rad/s, namely, that there is not much variation in the conductivity with Angular frequency over this range. as the Angular frequency is increased, σ_{ac} shows a monotonic increase following.Such dependence could be described by the variable range hopping (VRH) mechanism. This model is important for the electrical conduction mechanism.The whole curve can be fitted to the power law [32]:

$$\sigma_{ac}\omega = \sigma_{dc} + A\,\omega^{s} \quad \text{.....(1)}$$

Where σ_{dc} is dc conductivity, A is an arbitrary constant and s is frequency exponent, with 0 < s < 1.σ_{dc} can be obtained by extrapolating the low frequency plateau to zero frequency , and fit values of $\sigma_{dc}$and s, obtained are depicted in Table2. It can be seen that the Ac conductivity at low

frequency increase with temperature to attain a maximum of 7.85×10-5S/cm for a temperature of 353 K then it decreases with the augmentation of temperature. This trend of conductivity versus conductivity could be attributed to the degradation of cross-linking (TPGDA) chains by the thermal effect.It is clear from that all s values aretemperature dependent and less than unity [33] ,it is also observed that s decreases with increasing temperature, but starting with 433 K it increases.

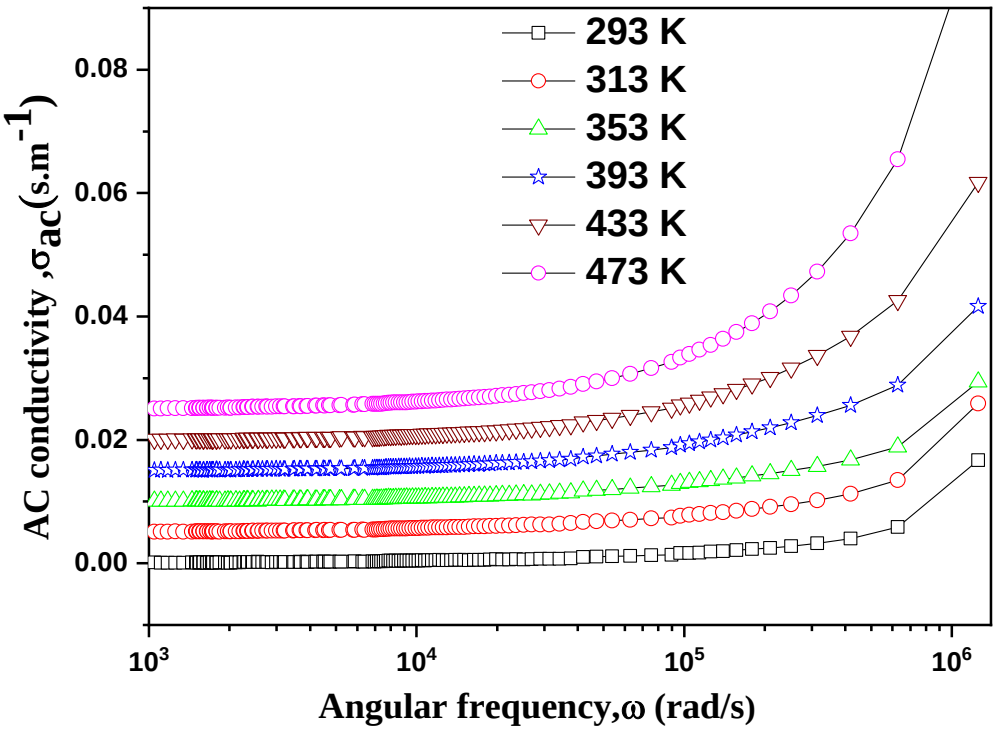

Figure 6. Ac conductivity spectra as function of angular frequency measured under various thermal conditions for the cross-linking (TPGDA)/MMt-Cs^+nanocomposite.

Table 2. Measured dc conductivity and frequency exponent (s)versus temperature (Kelvin) for the cross-linking (TPGDA)/MMt-Cs^+ nanocomposite samples.

T(K)	Conductivity (S cm^{-1})	s
293	1.01× 10-4	0.941
313	8.48× 10-5	0.817
353	7.85 × 10-5	0.779
393	-1.50 × 10-5	0.748

433	-4.46 × 10-5	0.791
473	-1.05 × 10-6	0.887

Fig. 7 show the Ac conductivity spectra as function of angular frequency measured at 313K for the (cross-linked (TPGDA)/MMt-M^+ nanocomposite. The values of σ_{dc} and s were extracted from previous equation (1) and the results are recorded in the Table 5.

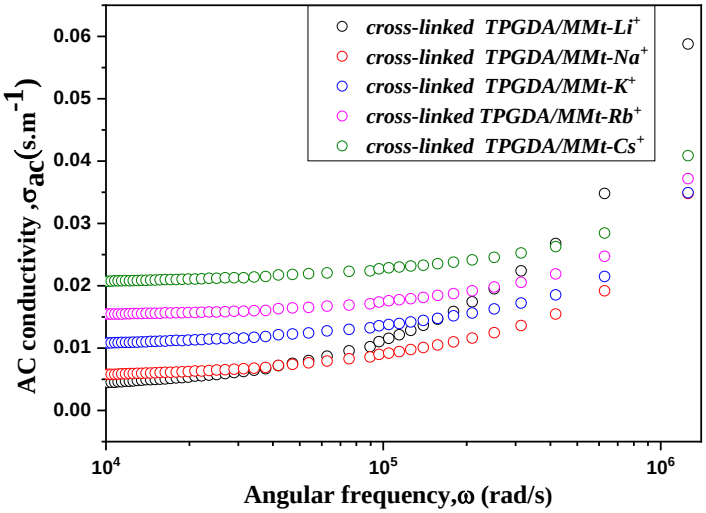

Figure 7. Ac conductivity spectra as function of angular frequency measured at 313K for the cross-linking (TPGDA)/MMt-M^+ nanocomposite.

Table 3. Measured dc conductivity and frequency exponent (s) for the cross-linking (TPGDA)/MMt-M^+nanocompositeat 313 K.

Samples	Conductivity(S cm^{-1})	S
cross-linking (TPGDA)/MMt-Li^+	4.59× 10-4	0.919
cross-linking (TPGDA)/MMt-Na^+	7.34× 10-5	0.811
cross-linking (TPGDA)/MMt-K^+	6.57 × 10-4	0.822
cross-linking (TPGDA)/MMt-Rb^+	4.55 × 10-5	0.909
cross-linking (TPGDA)/MMt-Cs^+	8.48× 10-5	0.817

Dielectric Analysisfor cross-linked (TPGDA)/MMt-Cs+nanocomposite

Dielectric Constant (ε′)

In Fig.8, the real part of permittivity (ε′) is shown as a function of frequency for the cross-linking (TPGDA)/MMt-Cs^{+} nanocomposite at different treatment temperatures. It was observed that the dielectric constant decreased at high frequencies as the frequency of the applied electric field increased. This can be attributed to the fact that the polarized superposition of material gains a dipole moment under the influence of the alternating external electric field, causing the charge carriers to accumulate and block the negative electrode. As a result, the charge of the vacuum decreases, leading to a decrease in capacitance and hence a decrease in dielectric constant.

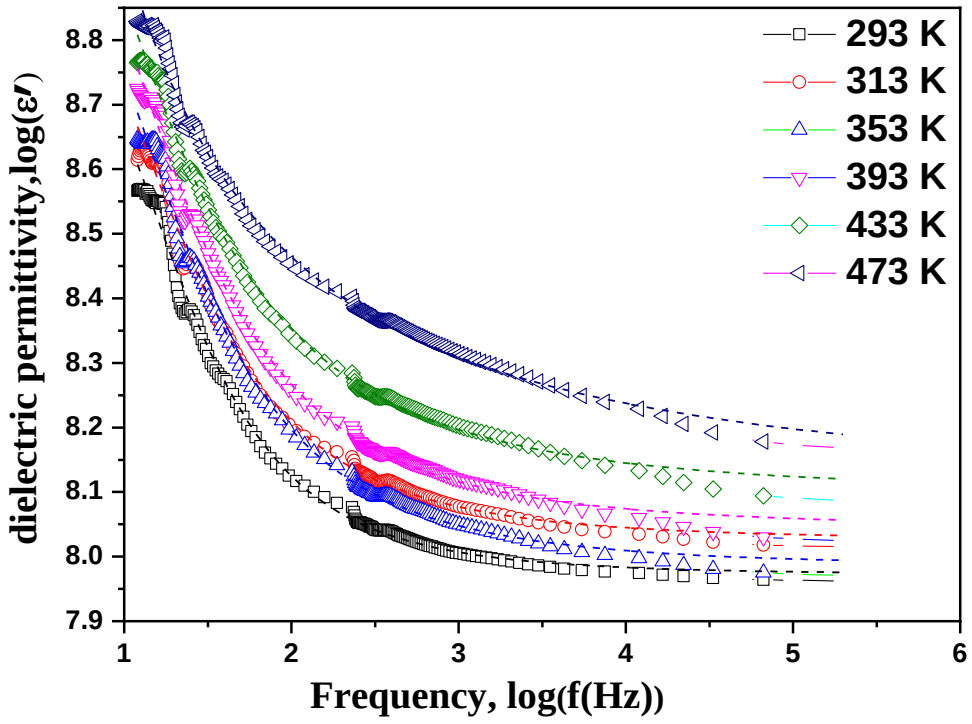

Figure 8. Real part of dielectric permittivity(ε′)versus frequency (in log-log scale) at different treatment temperatures in the case of the cross-linking (TPGDA)/MMt-Cs^{+} nanocomposite.

The alignment of dipoles in an insulation material is known to be influenced by temperature, with diodes exhibiting restricted rotation at low temperatures that becomes easier as temperature increases. This is reflected in an increase in the low-frequency-limit dielectric constant (ε_s) for the material, as observed in the results presented in Table 4. The calculation of extinction ε_s and

high-frequency limit dielectric constant (ε_∞) is accomplished through the use of equation 2, which includes fitting parameters such as ε_s, ε_∞, τ, α, and β. These parameters serve to determine the principal value of the relaxation time of the effective grain dipole rotation in the system and the dielectric distribution parameter, respectively.

$$\varepsilon = \varepsilon_\infty + \frac{\varepsilon_s - \varepsilon_\infty}{\left(1+(i\omega\tau)^{1-\alpha}\right)^{\beta}} \quad \ldots\ldots\ldots\ldots\ldots\ldots(2)$$

Table 4. The fitted dielectric parameters (ε_∞, ε_s) of the cross-linking (TPGDA)/MMt-Cs^+nanocomposite

Samples at	ε_∞	ε_s
293	7.972	8.868
313	7.975	8.914
353	7.884	8.927
393	7.894	10.709
433	7.897	9.007
473	7.840	9.122

Dielectric Loss (ε'')

Fig. 9 depicts the imaginary part of the dielectric permittivity as a function of frequency, plotted on a double logarithmic scale for the (TPGDA)/MMt-Cs^+ nanocomposite sample with varying temperatures. The plot exhibits a series of straight lines with differing slopes. The high dielectric loss observed at low frequencies is attributed to free charge motion within the material. The increase in ε'' at lower frequencies is indicative of enhanced charge carrier mobility. At higher frequencies, the dielectric loss decreases and becomes independent of temperature, indicating that charge carriers are unable to keep pace with the electric field. This phenomenon may arise due to the relaxation time of the charge carriers being shorter than the time period of the applied electric field.

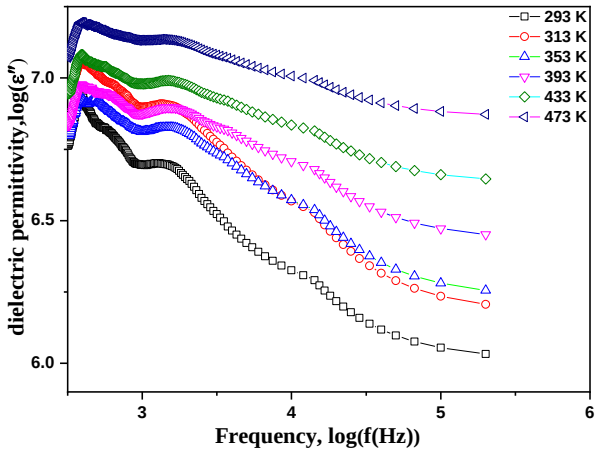

Figure 9. Imaginary part of dielectric permittivity (ε″) versus frequency (in log-log scale) at different treatment temperatures in the case of the cross-linking (TPGDA)/MMt-Cs⁺ nanocomposite.

Loss tangent (tan)

Fig. 10 illustrates the variation of tangent loss (tanδ) as a function of frequency for the cross-linking (TPGDA)/MMt-Cs⁺nanocomposite treated at different temperatures. At a constant temperature, the values of the loss factor increase as frequency increases, reaching their maximum at phase-reversal points before decreasing sharply. The peak in the tangent loss arises due to relaxation within the material, which can be attributed to the relaxation time of the charge carriers.

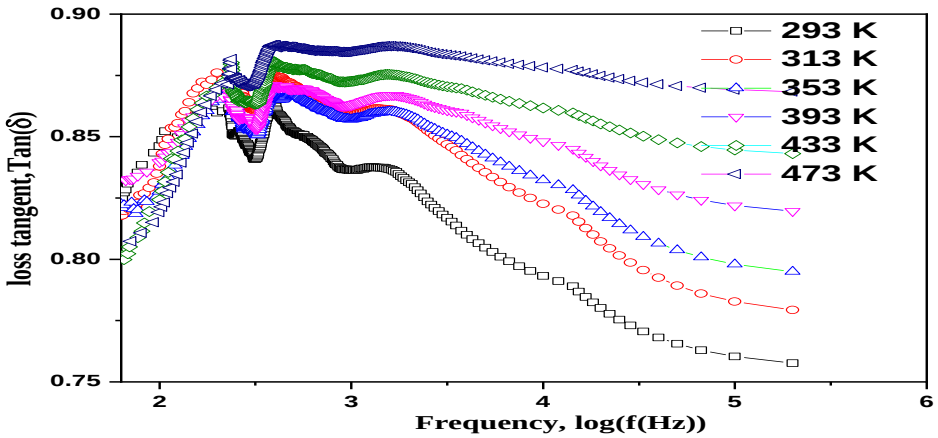

Figure 10. Loss tangent (tanδ) versus frequency (in log scale) for the cross-linking (TPGDA)/MMt-Cs⁺nanocomposite.

Fig. 11 and Fig. 12display the real and imaginary parts of the dielectric permittivity, respectively, plotted on a log-log scale as a function of cation. The real part of the dielectric permittivity exhibits a trend that follows the ionic mobility of the cations. The values of ε_s and ε_∞ were obtained using Equation (2), and the results are presented in Table 5. The results show that the real permittivity increases with increasing cation binding as follows:

ε_s(cross-linked (TPGDA)/MMt-Li^+)>ε_s(cross-linked (TPGDA)/MMt-K^+)>ε_s(cross-linked (TPGDA)/MMt-Cs^+)>ε_s(cross-linked (TPGDA)/MMt-Na^+)>ε_s(cross-linked (TPGDA)/MMt-Rb^+).

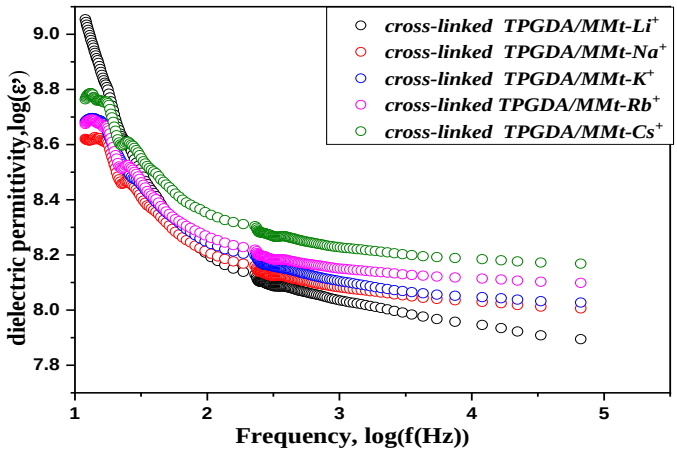

Figure 11. Real part of dielectric permittivity(ε′)versus frequency (in log-log scale)at 313K for the cross-linking (TPGDA)/MMt-M^+nanocomposite.

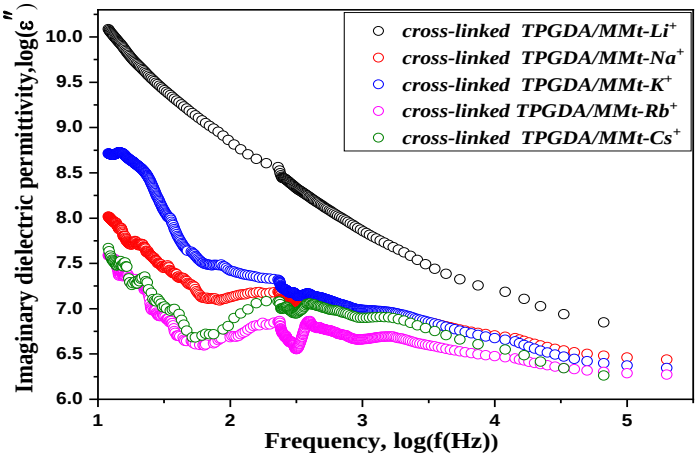

Figure 12. Imaginary part of dielectric permittivity (ε′′) versus frequency (in log-log scale) at 313K for cross-linking (TPGDA)/MMt-M^+nanocomposite.

Table 5. The fitted dielectric parameters (ε_∞, ε_s) at 313 K:

sample	ε_∞	ε_s
cross-linking (TPGDA)/MMt-Li^+	7.896	14.532
cross-linking (TPGDA)/MMt-Na^+	7.969	8.878
cross-linking (TPGDA)/MMt-K^+	7.922	9.082
cross-linking (TPGDA)/MMt-Rb^+	7.964	8.796
cross-linking (TPGDA)/MMt-Cs^+	7.975	8.914

Fig.13 depicts the variation of loss tangent (tanδ) as a function of frequency (log scale) for the (TPGDA)/MMt-M^+ nanocomposite at 313K. The dielectric loss pattern reveals a relaxation peak that shifts towards higher frequency after the introduction of different cations into the montmorillonite clay. This indicates a decrease in relaxation time, independent of clay concentration and temperature, and is a clear indication of faster ion dynamics. Specifically, the shift in relaxation peak is observed in the cross-linking (TPGDA)/MMt-Li^+ sample.

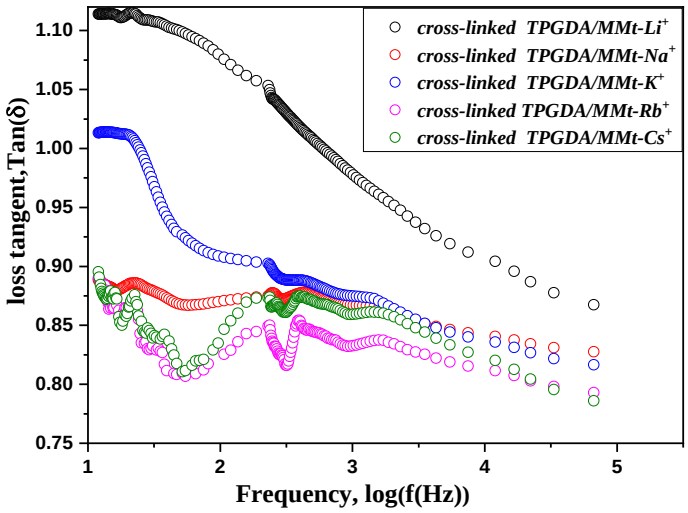

Figure 13. Loss tangent (tanδ) measured at 313K versus frequency (in log scale) for the cross-linking (TPGDA)/MMt-M^+nanocomposite.

Conclusion

The results of this study demonstrate the successful intercalation of montmorillonite layers by (TPGDA) as confirmed by XRD analysis. The IRTF analysis also showed the presence of new absorption bands attributed to the surfactant used and a decrease in the amount of water. The dielectric properties of cross-linking (TPGDA)/MMt-M^+ were investigated over a frequency range of 12Hz to 200 MHz and a temperature range of 293–473K. The results showed that the addition of TPGDA to the montmorillonite resulted in enhancements in AC conductivity (σ_{ac}), Dielectric Constant (ε′), tangent loss (tan), and Dielectric Loss (ε″) compared to the pure material. The study also found that the real part of dielectric permittivity followed the ionic mobility of the cations. The relaxation time was found to decrease with the addition of cations to the clay, indicating faster ion dynamics. These findings provide insights into the potential applications of cross-linking (TPGDA)/MMt-M^+ nanocomposites in various fields such as electronics and energy storage.

References

[1]. Okada, A., &Usuki, A. The chemistry of polymer-clay hybrids. *Materials Science and Engineering*: C, 3(2), 109-115. DOI: 10.1016/0928-4931(95)00110-7.

[2]. Reynaud, E., Jouen, T., Gauthier, C., Vigier, G., & Varlet, J. Nanofillers in polymeric matrix: a study on silica reinforced PA6. *Polymer* **2001**, 42(21), 8759-8768. DOI: 10.1016/S0032-3861(01)00446-3.

[3]. Yang, F., & Nelson, G. L.PMMA/silica nanocomposite studies: synthesis and properties. *Journal of applied polymer science* **2004**, 91(6), 3844-3850.DOI: 10.1002/app.13573.

[4]. Gilman, J. W. Flammability and thermal stability studies of polymer layered-silicate (clay) nanocomposites. *Applied clay science***1999**, 15(1-2), 31-49.DOI: 10.1016/S0169-1317(99)00019-8.

[5]. Wang, S., Hu, Y., Zong, R., Tang, Y., Chen, Z., & Fan, W. Preparation and characterization of flame retardant ABS/montmorillonitenanocomposite. *Applied Clay Science***2004**, 25(1-2), 49-55.DOI: 10.1016/j.clay.2003.08.003.

[6]. Wan, M., & Li, J. Synthesis and electrical–magnetic properties of polyaniline composites. *Journal of Polymer Science Part A: Polymer Chemistry***1998**, 36(15), 2799-2805.DOI: 10.1002/(SICI)1099-0518(19981115)36:15<2799::AID-POLA17>3.0.CO;2-1.

[7]. Zheng, W., Wong, S. C., & Sue, H. J. Transport behavior of PMMA/expanded graphite nanocomposites. *Polymer***2002**, 43(25), 6767-6773.DOI: 10.1016/S0032-3861(02)00599-2.

[8]. Barnakov, Y. A., Scott, B. L., Golub, V., Kelly, L., Reddy, V., & Stokes, K. L. Spectral dependence of Faraday rotation in magnetite-polymer nanocomposites. *Journal of Physics and Chemistry of Solids* **200**4, 65(5), 1005-1010.DOI: 10.1016/j.jpcs.2003.10.070.

[9]. Wan, M., & Fan, J. Synthesis and ferromagnetic properties of composites of a water-soluble polyaniline copolymer containing iron oxide. *Journal of Polymer Science Part A: Polymer Chemistry***1998**, 36(15), 2749-2755. DOI:10.1002/(SICI)1099-0518(19981115)36:15<2749::AID-POLA11>3.0.CO;2-O.

[10]. Madejová, J., Arvaiová, B., &Komadel, P. FTIR spectroscopic characterization of thermally treated Cu^{+2}, Cd^{+2}, and Li^{+}montmorillonites. *SpectrochimicaActa Part A: Molecular and Biomolecular Spectroscopy***1999**, 55(12), 2467-2476.DOI: 10.1016/S1386-1425(99)00039-6.

[11]. Tyagi, B., Chudasama, C. D., &Jasra, R. V.Determination of structural modification in acid activated montmorillonite clay by FT-IR spectroscopy. *SpectrochimicaActa Part A: Molecular and Biomolecular Spectroscopy* **2006**, 64(2), 273-278.DOI: 10.1016/j.saa.2005.07.018.

[12]. Kubranová, M., Jóna, E., Rudinská, E., Nemceková, K., Ondrušová, D., &Pajtášová, M. Thermal properties of Co-, Ni-and Cu-exchanged montmorillonite with 3-hydroxypyridine. *Journal of thermal analysis and calorimetry***2003**, 74(1), 251-257.DOI:10.1023/A:1026350424642.

[13]. Z. Radojevic, A. Mitrovic, *Journal of the European Ceramic Society***2007**, 27,1691–1695.

[14]. Miranda, R., Ríos, H., Delgado, F., Castro, M., Cogordán, A., &Salmón, M. Characterization of a bentonitic clay and its application as catalyst in the preparation of benzyltoluenes and oligotoluenes. *Applied Catalysis A: General***2003**, 244(2), 217-233.DOI: 10.1016/S0926-860X(02)00566-5.

[15]. Peker, S., Yapar, S., &Beşün, N. Adsorption behavior of a cationic surfactant on montmorillonite. *Colloids and Surfaces A: Physicochemical and Engineering Aspects***1995**, 104(2-3), 249-257.DOI: 10.1016/0927-7757(95)03280-8.

[16]. López-Galindo, A., Viseras, C., &Cerezo, P.Compositional, technical and safety specifications of clays to be used as pharmaceutical and cosmetic products. *Applied Clay Science***2007**, 36(1-3), 51-63. DOI: 10.1016/j.clay.2006.06.016.

[17]. An, N., Zhou, C. H., Zhuang, X. Y., Tong, D. S., & Yu, W. H. Immobilization of enzymes on clay minerals for biocatalysts and biosensors. *Applied Clay Science***2015**, 114, 283-296. DOI: 10.1016/j.clay.2015.05.029.

[18]. Tunç, S., &Duman, O. Preparation and characterization of biodegradable methyl cellulose/montmorillonitenanocomposite films. *Applied Clay Science***2010**, 48(3), 414-424.DOI: 10.1016/j.clay.2015.05.029.

[19]. Tunç, S., &Duman, O. Preparation of active antimicrobial methyl cellulose/carvacrol/montmorillonitenanocomposite films and investigation of carvacrol

release. *LWT-Food Science and Technology***2011**, 44(2), 465-472.DOI: 10.1016/j.lwt.2010.08.018.

[20]. Tunc, S., Duman, O., &Polat, T. G. Effects of montmorillonite on properties of methyl cellulose/carvacrol based active antimicrobial nanocomposites. *Carbohydrate polymers***2016**, 150, 259-268. DOI: 10.1016/j.carbpol.2016.05.019.

[21]. Duman, O., Tunc, S., &Polat, T. G. Adsorptive removal of triarylmethane dye (Basic Red 9) from aqueous solution by sepiolite as effective and low-cost adsorbent. *Microporous and Mesoporous Materials***2015**, 210, 176-184. DOI: 10.1016/j.micromeso.2015.02.040.

[22]. Duman, O., Tunç, S., &Polat, T. G. Determination of adsorptive properties of expanded vermiculite for the removal of CI Basic Red 9 from aqueous solution: kinetic, isotherm and thermodynamic studies. *Applied Clay Science***2015**, 109, 22-32.DOI: 10.1016/j.clay.2015.03.003.

[23]. Tunç, S., Duman, O., &Kancı, B. Rheological measurements of Na-bentonite and sepiolite particles in the presence of tetradecyltrimethylammonium bromide, sodium tetradecylsulfonate and Brij 30 surfactants. *Colloids and Surfaces A: Physicochemical and Engineering Aspects***2012**, 398, 37-47. DOI: 10.1016/j.colsurfa.2012.02.006.

[24]. (http://www.uv-curing-monomer.com/Products/Tripropylene-Glycol-Diacrylate.htm).

[25]. For further information on this substance or product safety summary in general, please contact: ICCA portal where the GPS Safety Summary is posted:http://www.icca chem.org/en/Home/ICCA-initiatives/global-product-strategy/

[26]. Berend, I. The mechanisms of hydration of homoionicmontmorillonites for relative pressures lower than 0.95 (Doctoral dissertation, National Polytechnic Institute of Lorraine) **1991**.

[27]. Madejová, J. FTIR techniques in clay mineral studies. *Vibrational spectroscopy***2003**, 31(1), 1-10.DOI: 10.1016/S0924-2031(02)00065-6.

[28]. dos Santos, V. C. G., Grassi, M. T., & Abate, G.Sorption of Hg (II) by modified K10 montmorillonite: influence of pH, ionic strength and the treatment with different cations. *Geoderma***2015**, 237, 129-136.DOI: 10.1016/j.geoderma.2014.08.018

[29]. Sposito, G., Prost, R., &Gaultier, J. P. Infrared spectroscopic study of adsorbed water on reduced-charge Na/Li-montmorillonites. *Clays and clay minerals***1983**, 31(1), 9-16.DOI: 10.1346/CCMN.1983.0310102

[30]. Wu, P., Wu, W., Li, S., Xing, N., Zhu, N., Li, P., ...& Dang, Z. Removal of Cd^{+2} from aqueous solution by adsorption using Fe-montmorillonite. *Journal of Hazardous Materials***2009**, 169(1-3), 824-830.DOI: 10.1016/j.jhazmat.2009.04.022.

[31]. Wu, L., Yang, C., Mei, L., Qin, F., Liao, L., &Lv, G. Microstructure of different chain length ionic liquids intercalated into montmorillonite: a molecular dynamics study. *Applied clay science***2014**, 99, 266-274.DOI: 10.1016/j.clay.2014.07.004.

[32]. Jonscher, A. K., Dielectric Relaxation in Solids, Press: Chelsea Dielectrics, London, **1983**; 380 pp.

[33]. Yoshimoto, S., Ohashi, F., &Kameyama, T. Simple preparation of sulfate anion-doped polyaniline-clay nanocomposites by an environmentally friendly mechanochemical synthesis route. *Macromolecular rapid communications***2004**, 25(19), 1687-1691.DOI: 10.1002/marc.200400299

Acknowledgment

The samples were meticulously prepared in the physics laboratory located at MabroukiNouari in DjebelMessaad, M'sila, Algeria. was made possible thanks to the expertise of HakimaAit Youssef from the Emerging Materials Unit at the University of Setif, Setif, Algeria. The authors would like to express their utmost gratitude to the reviewers for their invaluable comments and suggestions, which greatly enhanced the quality of this work.

Conflict of Interest and Authorship Conformation Form

- All authors have participated in (a) conception and design, or analysis and interpretation of the data; (b) drafting the article or revising it critically for important intellectual content; and (c) approval of the final version.
- This manuscript has not been submitted to, nor is under review at, another journal or other publishing venue.
- The authors have no affiliation with any organization with a direct or indirect financial interest in the subject matter discussed in the manuscript